Mode-matched InP Waveguides For Low-Loss Fiber-Chip Butt Coupling

A. Pohl[1] and H. Fouckhardt[2]

1) with Furukawa Industrial S.A.
Rua Hasdrubal Bellegard, 820
81450-140 - Curitiba - Pr - Brazil

2) with Institut fuer Hochfrequenztechnik
Postfach 3329 - Techn. Univ. Braunschweig
D-38023 Braunschweig Germany

Recebido em 16 de Outubro, 1995

Neste artigo relatamos o procedimento de cálculo e a fabricação de guias de onda de entrada em InP para circuitos de fotônica integrada. Os guias de onda são fabricados por meio das técnicas de epitaxia de fase líquida (LPE) e de corrosão química úmida (WET). Uma estrutura de guia de onda simétrica é também apresentada como alternativa às seções transversais de guias de onda convencionais, com a finalidade de melhorar o acoplamento óptico com fibras ópticas monomodo. Uma atenuação de 0.7 dB/interface entre os modos fundamentais do guia de onda e de uma fibra monomodo com 9 μm de diâmetro modal pôde ser obtida experimentalmente.

We report on the design and fabrication of mode-matched InP waveguides produced with liquid phase epitaxy (LPE) and wet chemical etching (WET), which serve as input waveguides for integrated photonic circuits. A new symmetric waveguide structure is presented as an alternative to ordinary waveguide cross-sections for butt coupling purposes. Mismatch loss of 0.7 dB/interface to a single-mode fiber with 9 μm spot diameter has been achieved experimentally.

1. Introduction and Waveguide Concept

Efficient low-cost and robust fiber-chip connections with large alignment tolerances are essential for practical applications of integrated photonics in communication systems. However, losses are mainly due to the large mismatch between the mode size of a standard single-mode fiber ($8-10\,\mu$m) and the small size of the mode in the chip waveguide ($\approx 1\,\mu$m). Fresnel reflections on the interface also contribute strongly to the coupling losses due to the different refractive indices of the glass fiber and of III-V semiconductor materials, which generally forces the use of antireflection coatings. Among several approaches that have been presented to solve the problem, the spot-size transformation technique on chip offers the advantage of large alignment tolerances, long-term stability, and suitability for mass production. By this technique the usual mode field of a standard single-mode fiber is first matched to a large input waveguide that is then connected to the small chip waveguide via a nested integrated optical taper [1].

The design of input waveguides for optimum mode matching points to structures with approximately square cross-section of large width and depth comparable to the size of the fiber core [2]. The simplest realization of such a structure is a rib waveguide (see Fig. 1a.) with a large film thickness ($8-9$ μm), a deeply etched side wall (>5 μm) and a small refractive index difference ($\Delta n \approx 3\times10^{-3}$) between guiding layer and cladding to obtain a large fundamental mode size. A symmetrical structure presents an alternative approach, which avoids the difficulty in etching very deep side walls. In this case an inverted rib (a groove) is etched into a substrate or a buffer layer and covered with a thick epitaxial film, which is then patterned to obtain a rib just above the inverted one (see Fig. 1b). Both structures may be overgrown in a second epitaxial step to lower the waveguide core-cover index step and further widen the guided mode size. Here we report on the design of these fiber matched InP waveguides assuming small carrier concentration changes in n^-/n^+ layers and their fabrication [3]. Besides the achievement of very small refractive index differences, low losses may be expected if slight carrier doping is employed. An estimate gives values for waveguide propagation losses of less than 2.4 dB/cm for a doping level of 2.0×10^{17} cm^{-3}, which will be acceptable if input waveguides are no longer than 1 mm. The waveguides were designed using the finite difference method and fabricated using liquid phase epitaxy and wet chemical etching. Moreover we show experimental results concerning the overlap efficiency to the fundamental fiber mode and trace a comparison with results from the literature.

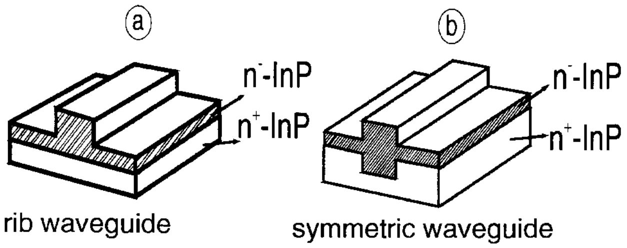

Figure 1 - Schematic representation of an input a) rib waveguide, b) symmetric waveguide.

2. Excitation efficiency for butt joints

The task of optimizing the coupling between a single-mode fiber and an input waveguide requires the calculation of the excitation efficiency, showing how much power of the incident fiber mode couples into one excited mode of the waveguide. To calculate this efficiency we expand the incident fundamental fiber mode at the interface into the guided modes ($\nu = 0, \ldots, \mu, \ldots, N$) of the input waveguide. By matching the transversal field components one obtains:

$$\mathbf{E_t}_f + r\,\mathbf{E_t}_f = \sum_{\nu=0}^{N} a_\nu \mathbf{E_t}_\nu, \quad (1)$$

$$\mathbf{H_t}_f - r\,\mathbf{H_t}_f = \sum_{\nu=0}^{N} a_\nu \mathbf{H_t}_\nu. \quad (2)$$

$\mathbf{E_t}_f$ and $\mathbf{H_t}_f$ on the left side of Eqs. (1) and (2) represent, respectively, the transversal electric and magnetic components of the fundamental fiber mode in the forward direction together with their parts reflected at the step backwards; r denotes the amplitude reflection coefficient. $\mathbf{E_t}_\nu$ and $\mathbf{H_t}_\nu$ on the right side are the transversal field components of the guided modes in the input waveguide, where a_ν represents the unknown amplitudes to be determined. We neglect the radiation modes in the model by assuming a very small step at the interface in the calculations. Yet one may consider their influence roughly by calculating a power balance using the normalized reflection and forward amplitude coefficients, as suggested in [4]. To obtain the excitation coefficient a_μ of a certain mode μ of the waveguide, we take the vector product of Eqs. (1) and (2) with the complex conjugate of the transversal field components $\mathbf{E}^*_\mu$ and $\mathbf{H}^*_\mu$ of that mode. Integrating both equations over the total cross-section we have

$$(1+r)\iint_{-\infty}^{+\infty}(\mathbf{E_t}_f \times \mathbf{H^*_t}_\mu)\,\mathrm{d}x\,\mathrm{d}y = \sum_{\nu=0}^{N} a_\nu \iint_{-\infty}^{+\infty}(\mathbf{E_t}_\nu \times \mathbf{H^*_t}_\mu)\,\mathrm{d}x\,\mathrm{d}y \quad (3)$$

$$(1-r)\iint_{-\infty}^{+\infty}(\mathbf{H_t}_f \times \mathbf{E^*_t}_\mu)\,\mathrm{d}x\,\mathrm{d}y = \sum_{\nu=0}^{N} a_\nu \iint_{-\infty}^{+\infty}(\mathbf{H_t}_\nu \times \mathbf{E^*_t}_\mu)\,\mathrm{d}x\,\mathrm{d}y. \quad (4)$$

Taking the orthogonality relations of the normalized eigenmodes into account, all terms with $\nu \neq \mu$ will fall off. Eliminating r from the resulting equations we obtain the following relation for the excitation coefficient a_μ:

$$a_\mu = 2\,\frac{\iint_{-\infty}^{+\infty} (\mathbf{E_{t}}_f \times \mathbf{H^*_{t}}_\mu)\,\mathrm{d}x\,\mathrm{d}y \iint_{-\infty}^{+\infty} (\mathbf{E^*_{t}}_\mu \times \mathbf{H_{t}}_f)\,\mathrm{d}x\,\mathrm{d}y}{\iint_{-\infty}^{+\infty} (\mathbf{E_{t}}_\mu \times \mathbf{H^*_{t}}_\mu)\,\mathrm{d}x\,\mathrm{d}y \iint_{-\infty}^{+\infty} (\mathbf{E^*_{t}}_\mu \times \mathbf{H_{t}}_f)\,\mathrm{d}x\,\mathrm{d}y + \iint_{-\infty}^{+\infty} (\mathbf{E_{t}}_\mu \times \mathbf{H_{t}}_\mu)\,\mathrm{d}x\,\mathrm{d}y \iint_{-\infty}^{+\infty} (\mathbf{E_{t}}_f \times \mathbf{H^*_{t}}_\mu)\,\mathrm{d}x\,\mathrm{d}y}\,. \tag{5}$$

The eigenmodes are normalized to unit power and the coefficient $\eta_\mu = |\, a_\mu\,|^2$ directly represents the fraction of power that is transmitted from the fiber into the guided mode of order μ. For optimization purposes we consider only the fundamental mode of the fiber (HE_{11}) and that of the input waveguide (HE_{00}). We neglect the index μ from now on and use only η. It seems convenient at this place to estimate an upper limit for η. This may be done assuming an ideal field overlap between both fundamental modes. Decomposing the vector products in Eq. (5) we obtain the following relation for the excitation efficiency:

$$\eta = \left| 4\,\frac{\iint_{-\infty}^{+\infty} (E_{xw}H_{yf} - E_{yw}H_{xf})\,\mathrm{d}x\,\mathrm{d}y \iint_{-\infty}^{+\infty} (E_{xf}H_{yw} - E_{yf}H_{xw})\,\mathrm{d}x\,\mathrm{d}y}{\iint_{-\infty}^{+\infty} (E_{xw}H_{yf} - E_{yw}H_{xf} + E_{xf}H_{yw} - E_{yf}H_{xw})\,\mathrm{d}x\,\mathrm{d}y} \right|^2 , \tag{6}$$

where the indices f and w indicate the fiber and the input waveguide, respectively. Assuming that $H_y >> H_x$ for the HE_{00} mode of the input waveguide and introducing the relationship $E_x = (\beta/(\omega\epsilon))\,H_y = (\beta/(\kappa\epsilon_r))\sqrt{(\mu_0/\epsilon_0)}\,H_y$ it is possible to write Eq. (6) in the form

$$\eta = \left| 2\,\frac{\beta_w\beta_f}{\beta_w\,\epsilon_{r,f} + \beta_f\,\epsilon_{r,w}}\,\frac{\lambda}{\pi}\,\sqrt{(\mu_0/\epsilon_0)} \iint_{-\infty}^{+\infty} H_{yw}H_{yf}\;\mathrm{d}x\,\mathrm{d}y \right|^2 , \tag{7}$$

where

β_w: propagation constant of the HE_{00} mode;

β_f: propagation constant of the fiber HE_{11} mode;

$\epsilon_{r,w}$: relative dielectric constant of the input waveguide guiding region;

$\epsilon_{r,f}$: relative dielectric constant of the fiber core.

If we set $H_{yw} \approx H_{yf}$ in Eq. (7) and consider the normalization relation

$$2\,(\beta/(\kappa\epsilon_r))\sqrt{(\mu_0/\epsilon_0)} \iint_{-\infty}^{+\infty} H_y^2\,\mathrm{d}x\,\mathrm{d}y = 1 \tag{8}$$

for the guided modes and the fact that the effective index $N_{eff} = \beta/\kappa$ is approximately equal to the refractive index of the guiding region $n = \sqrt{\epsilon_r}$ in the case of a well guided fundamental mode, we will obtain following expressions for η

$$\eta_f = \left|\frac{2\,N_f}{N_f + N_w}\right|^2 \text{ or } \eta_w = \left|\frac{2\,N_w}{N_f + N_w}\right|^2 , \tag{9}$$

when for the sake of approximation either (β/ϵ_r) equals $(\beta_f/\epsilon_{r,f})$ or $(\beta_w/\epsilon_{r,w})$ in Eq. 8 for the fiber and the input waveguide, respectively. In the above formulae N_f and N_w mean the effective indices of the fundamental mode in the fiber and in the chip-waveguide, respectively. In this case, the upper limit for η will be given by the geometric average of both expressions above. So we have

$$\eta_{max} = \sqrt{\eta_f\,\eta_w} = 4\,\frac{|N_f\,N_w|}{|N_f + N_w|^2}\,, \tag{10}$$

which is only a function of the effective indices of the guides. This expression gives the maximum value possibly reached by the excitation efficiency and forms a guideline to optimize the field matching. As a rough estimate we substitute the values for the refractive index of the fiber core ($n_f = 1.453$) and that for the waveguiding layer of the input waveguide ($n_w = 3.205$) in the above formula and get a value of 86 % for η in this best case. In other words, by an ideal overlap of both fundamental modes, 14 % will be lost due to reflection on the interface. This is the same figure one gets by substituting the refractive indices in the Fresnel formula for plane waves at normal incidence.

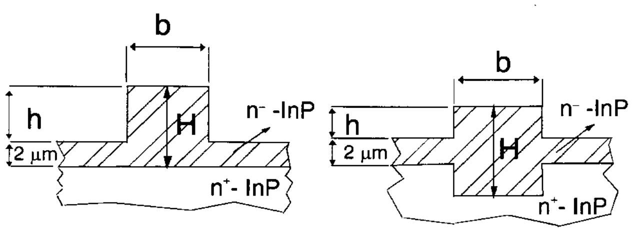

Figure 2 - Schematic representation of the cross-section of the input waveguides, showing the parameters used in the calculation. The film thickness $(H - h)$ besides the rib is fixed to 2 μm and a refractive index of $n_f = 3.205$ was estimated for the undoped InP film. The calculations were done varying the rib width b, the rib height h, and the total height H and considering buried and unburied guides.

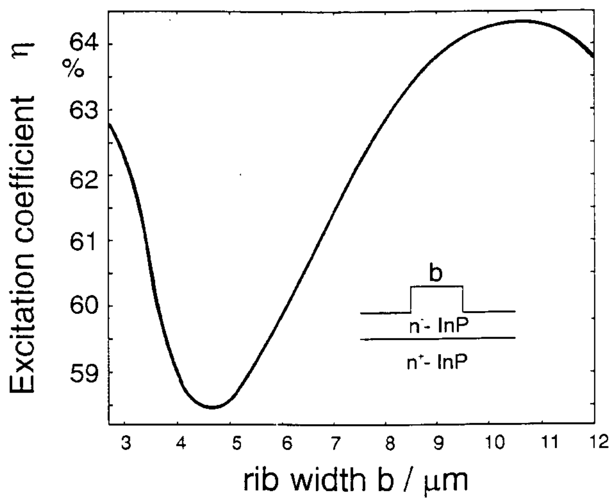

Figure 3 - Calculated excitation efficiency η of a rib waveguide as a function of the rib width b, where $h = 2$ μm and $\Delta n = 6.8 \times 10^{-3}$ between film and substrate.

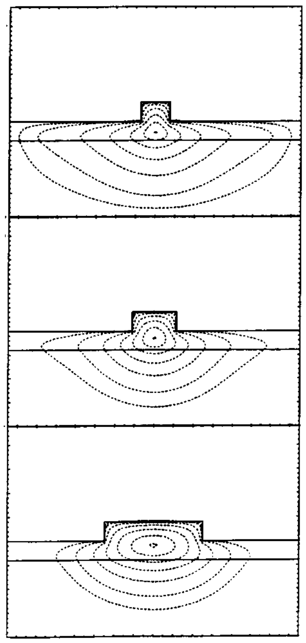

Figure 4 - Field contours of the rib waveguide of Fig. 3 calculated as a function of the following rib widths: a) $b = 3.0\,\mu$m, b) $b = 4.6\,\mu$m und c) $b = 10\,\mu$m. The curves represent contours of the magnetic field H_y with a 0.04, 1, 3, 6, 10, 15 and 20 dB decay.

To obtain the coefficient η we must first calculate the fundamental field modes of the fiber and the input waveguide. Due to the impossibility of obtaining an analytical solution for the waveguide equations, we attempted a numerical solution using a finite difference method, which is described in detail in [5]. The field distributions so obtained are substituted in Eq. (5) and integrated over the cross-section. A standard single-mode fiber [6] with a 9 μm spot diameter at $\lambda = 1.3\,\mu$m was used for the calculations. As a start point for the optimization one must consider an unconventionally large input structure to obtain a large mode size for matching with that of the fiber. The optimization task consists, starting from an ordinary chip-waveguide, in varying its dimensions and refractive index until a maximum for the excitation coefficient η is reached, while maintaining the fiber parameters constant. Due to the mutual dependence of the several design parameters and their contribution to the mode size we decided to fix some of them and let others vary. Under these circumstances we initially focused the attention to a rib waveguide and as a starting point set the film thickness, the rib width and rib height to be equal to 2 μm and let the rib width and then rib height vary (see Fig. 2 for the relevant parameters). The refractive index step between the guiding layer and the substrate is initially set to $\Delta n = 6.8 \times 10^{-3}$, which can be obtained through a light n-doping of the substrate under consideration of the several carrier-induced refractive index changes described in [7].

Figure 3 shows the variation of η as a function of the rib width b. The interesting behavior of this curve can be explained by looking at the field contours of Fig. 4. For small rib widths ($\leq 4\,\mu$m) we have a weak guiding effect, so that the magnetic field largely expands in the substrate and contributes in this way to a better matching with the fiber. At $b = 4.6\,\mu$m the field shrinks due to a better guidance in the waveguide and the curve reaches a minimum. Larger rib widths contribute again to an increase of the excitation efficiency based exclusively on the enlarged sizes of the structure. A maximum is obtained at $b = 10\,\mu$m. Fixing the rib width at this value we let the rib height h vary. The result can be seen in Fig. 5. The curves represent the behavior of η for the cases of an uncovered ($n_c = 1.0$) and a totally buried waveguide. The burying of the structures increases the excitation efficiency by enlargement of the mode size in the cover layer. In our case the excitation efficiency was computed considering the same refractive index for the substrate and the top layer. Moreover, an improvement of the excitation efficiency is observed for an increase of the substrate refractive index ($n_s = 3.198 \rightarrow n_s = 3.200$), which means a shrinkage of the refractive index step between substrate and guiding film. In this case, the broken curve of Fig. 5 shows that a maximum value of almost 84.5 % is obtained for $h = 6.5\,\mu$m. A further increase of the refractive index above 3.200 in the substrate causes a drastic reduction of the excitation efficiency due to the breakdown of the guidance condition and the occurrence of radiation losses (leakage). This value of ca. 84.5 % comes very close to the estimated maximum of 86 % by using the refractive indices of the fiber and the input waveguide in Eq. (10), and points to an almost complete overlapping of both fundamental modes.

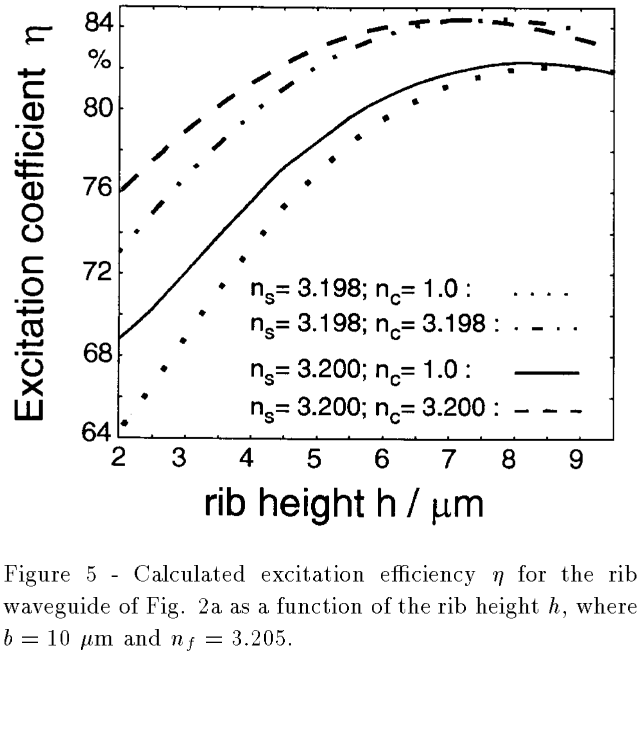

Figure 5 - Calculated excitation efficiency η for the rib waveguide of Fig. 2a as a function of the rib height h, where $b = 10\ \mu$m and $n_f = 3.205$.

A similar procedure is applied to the design of the symmetric input waveguide of Fig. 1b. In Fig. 6 we compare the excitation efficiency for both structures through the design parameter H (see Fig. 2), which describes the total structure height from substrate to the upper rib. For this computation a film thickness of 2 μm on the rib sides, a rib width of 10 μm and a refractive index of 3.200 in the substrate were considered in both structures. For uncovered waveguides ($n_c = 1.0$) the symmetric structure presents a better excitation efficiency for H above 6 μm. A cover layer with the same refractive index as that of the substrate ($n_s = n_c = 3.200$) improves η mainly for smaller values of H and practically no distinction can be made in the excitation efficiency curves of both waveguides.

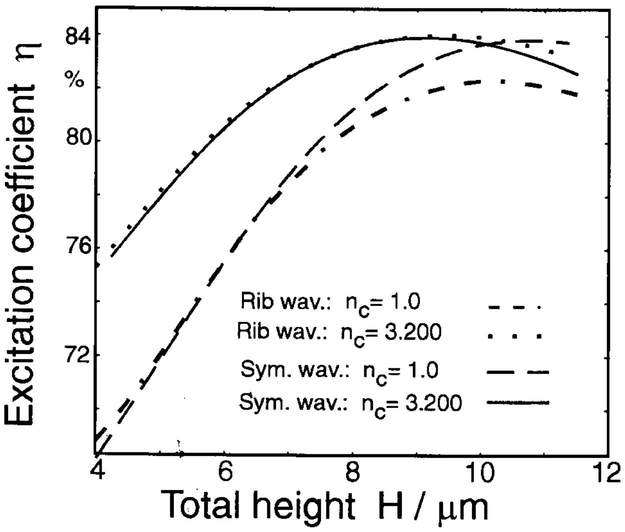

Figure 6 - Calculated excitation efficiency η of a rib and a symmetric waveguide calculated as a function of the total height H, where $b = 10\ \mu$m, $n_f = 3.205$ and $n_s = 3.200$. For the rib waveguide $H = h + 2\ \mu$m and for the symmetric waveguide $H = 2\,h + 2\ \mu$m.

The design of waveguides with such large cross-sections unfortunately allows the appearance of higher modes. A first theoretical investigation of this problem [8] resulted in very low excitation coefficients for *higher* modes only when the fiber is properly adjusted in front of the chip-waveguide.

3. Fabrication

As we have seen, the field matching to a fiber of spot size 9 μm requires waveguide structures with large cross-section dimensions, which impose constraints upon the fabrication process, mainly due to the difficulty with the deep wet etching of the rib side walls and epitaxial problems with the growth of a thick layer over a groove. However, using simple and well-known III-V solid-state technologies, such as the liquid phase epitaxy, optical lithography and wet chemical etching, we developed a technique to fabricate the input waveguides presented in Sec. 2 with good reproducibility.

The liquid phase epitaxy offers the advantage of high growth rates and the unique characteristic of planarization of grooved substrates. In the case of input rib waveguides a supercooling process has been used to grow a thick undoped n^--InP layer ($N_D \approx 1 \times 10^{16}$ cm^{-3}) from an In melt on [100] oriented S-doped InP planar substrates ($N_D \approx 3.75 \times 10^{18}$ cm^{-3}). The saturation and growth temperatures were 648 and 645°C, respectively, and the cooling rate was 0.5°C/min. Growth times longer than 35 min are needed to obtain layers thicker than 7 μm, as shown in Fig. 7. The broken curve represents an attempt to predict the layer thickness using Hsieh's diffusion model [9] of the growth process. The discrepancy arises due to an uncertain value of the diffusion coefficient assumed in the respective temperature interval during the computation. The solid curve was adjusted through the experimental points employing a least squares fit [10]. The fabrication of symmetric waveguides involves the etching of grooves in a planar substrate, which will be described further. A supercooling process was also used to grow a thick layer of undoped InP using the same 3°C difference between saturation and growth temperature and the same 0.5°C/min cooling rate. Yet a reduction of the growth temperature from 645 to 617°C was necessary to avoid a stronger decomposition of the grooved substrate due to Phosphor evaporation from the surface during the heat-up time. Since the growth rate on concave surfaces is larger than the rate on convex surfaces [11] it is possible to achieve a complete planarization of the grown film in relatively shallow etched substrates. Growth times no longer than 25 min were needed on 4 μm deep grooved substrates to obtain thick layers for the pattern of symmetric structures. For both structures an additional thin InGaAs layer was also grown on top of the undoped InP film in order to avoid surface degradation during the cooling phase. This layer was etched away in H_2SO_4 : H_2O_2 : H_2O (3:1:1) before the patterning step.

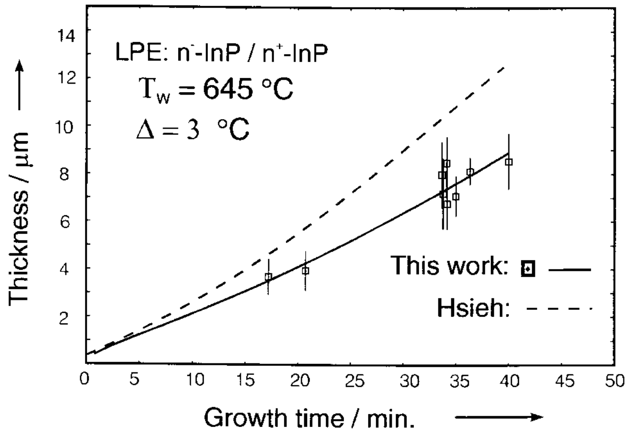

Figure 7 - Thickness of undoped InP-films as a function of the growth time. The solid curve shows a fitting to the experimental points. The broken curve is a growth estimate according to Hsieh [9].

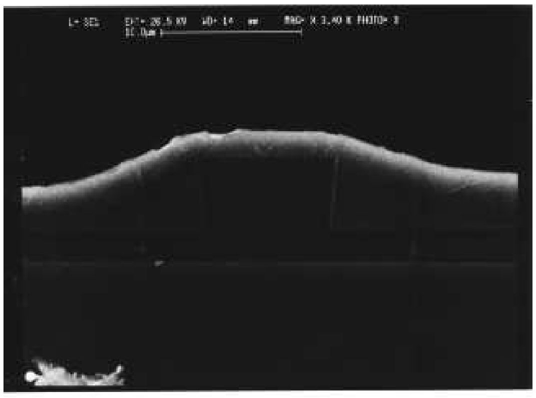

Figure 8 - SEM picture of an input rib waveguide.

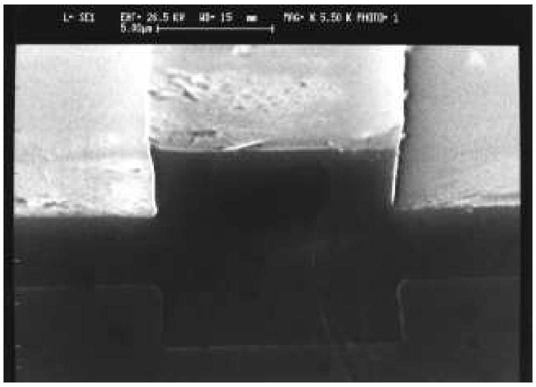

Figure 9 - SEM picture of an input symmetric waveguide.

Wet chemical etching was employed to pattern grooves and ribs on InP substrates. A crucial problem of wet chemical etching is the dependence of the wall profile on the cristallographic orientation and a number of process parameters. Usually it is not possible to get deep and steep side walls using photoresist as an etching mask. We developed a technique, where nearly vertical $(01\bar{1})$ and deep side walls for stripes placed along the [011] direction are obtained by using the combination of a Titanium mask and the etchant HCl : H_3PO_4. Input rib waveguides are fabricated by depositing a thin Titanium layer over the grown InP film and patterning with the photoresist AZ 1505 through ordinary optical lithography. The etch process in HCl : H_3PO_4 (1:3) follows at room temperature by moving the samples in the direction of the rib stripes. Two mask steps are needed to fabricate input symmetric waveguides also using the combination of a Titanium mask and the etchant above. In the first step the lift-off process is used to obtain inverted ribs in a InP substrate. The lift-off process will be necessary if the same lithographic mask is used in both mask steps, otherwise another mask with the inverted lithographic pattern should be used. The second masking step, after the epitaxy, is similar to the one used for fabricating rib waveguides. However the presence of underetching makes the width adjustment between ribs and grooves difficult. In [12] we presented a solution to this problem by tuning the photoresist exposure time during both masking procedures. Figures 8 and 9 show an SEM picture of a rib waveguide and of a symmetric waveguide, respectively. The rib waveguide is overgrown with a Sn-doped InP layer to improve the excitation efficiency, as observed in Sec. 2.

4. Measurements and Results

To evaluate the mode mismatch between the fiber and the input waveguide we use the near-field technique to measure the intensity distribution of the fundamental modes at the output of both waveguides. The intensity profile of the fiber is then fitted by a circular Gaussian of spot radius σ_0 in both vertical and lateral direction. In the chip waveguide the mode distribution is usually asymmetric and a Gaussian approximation is only good along the dimension parallel to the substrate. Yet a separable combination of Gaussian functions in the horizontal direction with spot size σ_3 and in the vertical direction with spot sizes σ_1 und σ_2 may be employed. This procedure is described in the literature [13, 12]. The substitution of these Gaussian approximations for the field distribution in the overlap coefficient

$$\eta' = \frac{\left| \int_{-\infty}^{\infty} \int_{-\infty}^{\infty} E_w(x,y) E_f^*(x,y)\, dx\, dy \right|^2}{\int_{-\infty}^{\infty} \int_{-\infty}^{\infty} \mid E_w(x,y) \mid^2 dx\, dy \int_{-\infty}^{\infty} \int_{-\infty}^{\infty} \mid E_f(x,y) \mid^2 dx\, dy} \tag{11}$$

leads to the following expression [14], which is only a function of the mode sizes:

$$\eta' = 2 \quad \frac{\left[\left(1/\sigma_0^2 + 1/\sigma_1^2\right)^{-1/2} + \quad \left(1/\sigma_0^2 + 1/\sigma_2^2\right)^{-1/2} \right]^2}{\sigma_0^2(\sigma_1 + \sigma_2)\sigma_3 \left(1/\sigma_0^2 + 1/\sigma_3^2\right)} \tag{12}$$

In practice we measured the intensity profiles of our waveguides separately along the vertical and horizontal directions and computed their spot radii, defined as the half width of the fitted Gaussian function at the $1/e^2$ point. A standard single-mode fiber with a mode diameter of 9 μm at $\lambda = 1.3\,\mu$m was used for the measurements. Its near-field was initially measured without the chip in the experimental arrangement. The sample bearing the input waveguides was then introduced into the set-up and the fundamental mode of the waveguide was excited by placing the fiber centered in front of its interface.

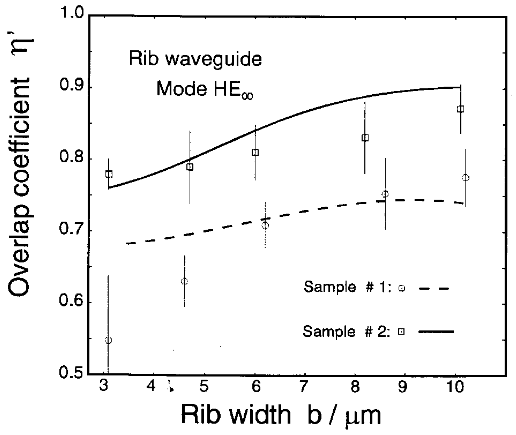

Figure 10 - Measured overlap coefficient η' of the HE_{00}-mode of input rib waveguides as a function of the rib width. The solid and broken curves show an estimate of η' computed with the finite difference method using parameters of the fabricated waveguides.

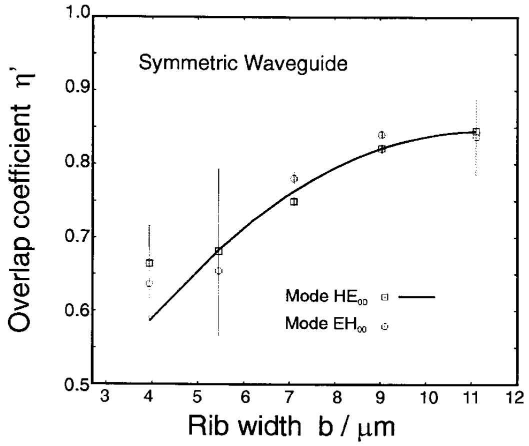

Figure 11 - Measured overlap coefficient η' of the HE_{00}- and EH_{00}-modes of an input symmetric waveguide as a function of the rib width. The solid line shows an estimate of η' for the HE_{00}-mode computed with the finite difference method.

Figure 10 shows results of the measured overlap coefficient η' for two input rib waveguides covered with a Sn-doped InP top layer as a function of the rib width b, where the same doping level was employed for the cover layer of both guides. Sample # 1 represents a rib waveguide with a film thickness of 1.9 μm on the rib sides ($d_{film} = H - h$) and $h = 2.1$ μm. A refractive index difference of $\Delta n \approx 1.3 \times 10^{-2}$ between substrate and guiding layer was estimated through the doping level in the substrate, that had been measured with the van der Pauw technique. Values for η' varying from 55 to 78 % are observed. Sample # 2 represents a similar structure with $h = 5.3$ μm and 2.0 μm on the rib sides. In this case the refractive index difference Δn was estimated to be $\Delta n \approx 3.5 \times 10^{-2}$. We observe values of the overlap coefficient η' varying from 78 till 87 % at a rib width of 10 μm. The solid and broken curves were calculated with the finite difference method considering the sample sizes and the nominal doping. A good approximation to the measured points is obtained in case of sample # 2, with the solid curve lying within the experimental error. For sample # 1 the approximation is good for large rib widths only, being quite poor for rib widths smaller than 5 μm. We attribute the discrepancies partially to the fact that the effective doping of the samples may have had different values than those assumed for the calculation. Another uncertainty concerns the cross-sectional dimensions of the samples, for an average has been assumed due to the thickness inhomogeneity of the grown film through the LPE.

Figure 11 shows results of the overlap coefficient for an input symmetric waveguide without a cover layer. The guide presents an average total height of $H = 7.6\,\mu$m, a film thickness of $d_{film} = 2.2$ μm besides the rib and a rib height (and groove depth) of $h = 2.7\,\mu$m. The refractive index step was estimated to be $\Delta n \approx 3.5 \times 10^{-2}$. The squares in Fig. 11 represent measured results for the HE_{00}-mode and the circles for the EH_{00}-mode of the input waveguide. Practically the same overlap is obtained in both cases, which demonstrates the symmetric character of the structure when compared to waveguides of smaller dimensions. The solid curve shows a theoretical comparison with the measured points for the HE_{00}-mode and it was also calculated with the finite difference method. A very good match to the experimental result is achieved. Overlap values from 66 to 85 % in the rib width range from 4 to 11 μm were obtained.

To compare these results with the theoretical predictions made in the beginning it is necessary to relate the measured overlap coefficient η' with the excitation coefficient η. This may be done through the simple approximated formula

$$\eta = \eta'(1 - R)\ , \tag{13}$$

which gives the coupling efficiency between the two waveguides and includes the reflection loss. $R = |r|^2$ means the reflectivity on the interface chip-waveguide/fiber and involves the knowledge of the effective refractive index of the propagated modes in both

Table 1: Estimated coupling efficiency of: 1) Rib waveguide with a Sn-doped cover layer (sample # 1); 2) Rib waveguide with a Sn-doped cover layer (sample # 2); 3) Symmetric waveguide without a cover layer.

Sample	Δn	Rib height (μm)	η
# 1	$1,3 \times 10^{-2}$	2,1	67 %
# 2	$3,5 \times 10^{-2}$	5,3	75 %
Sym. wav.	$3,5 \times 10^{-2}$	2,7	73 %

guides. η' gives the overlapping efficiency (field matching coefficient) between the guided modes and is calculated as shown above. The comparison has been done taking into account the overlap coefficient of an input waveguide of 10 μm rib width for all three samples presented. Assuming approximately a reflectivity of $R = 0.14$ in the interface fiber-chip, as seen in Sec. 2, we obtain values for η as presented in Table 1, which are 11 to 19 % under the maximum estimated figure of 86 % for waveguides without an anti-reflection coating.

The quite large refractive index difference Δn employed is responsible for the lower overlap results and is based on the fact that only market available InP-substrates with still relatively large S-doping ($\approx 10^{18}$ cm^{-3}) could be used for fabricating the input waveguides. A comparison to literature will be possible if we consider again the overlapping coefficient η'. Yet we limited our comparison to InGaAsP/InP-based waveguides butt-coupled to fibers with a spot diameter in the 8 to 10 μm range. Table 2 shows the results.

Table 2: Overlap efficiency η' for structures reported recently in the literature.

Reference	λ/μm	$2\sigma_0/\mu$m	Material	η'
Kasaya et al [15]	1,55	9	InGaAsP/InP	81 %
Zengerle et al [16]	1,55	8	InGaAsP/InP	$\geq$80%
Deri [17]	1,54	10	InGaAsP/InP(MQW)	95 %
This work	1,31	9	n^-/n^+-InP	85 %

The best one, as far as we know, achieves an overlap of $\eta' = 95$ % to a 10 μm spot-diameter single-mode fiber using a MQW-waveguide structure [17]. Our best result shows an overlap of 85 % and ranks among values reported recently by other authors. Figure 12 shows measured near-field profiles of the employed single-mode fiber (left) and of an input rib waveguide with 85 % overlap to the fiber field (right). Propagation losses for some of the fabricated input waveguides were also measured using the cut-back technique [18] at $\lambda = 1.3\,\mu$m. Lowest values of about 4 dB/cm were achieved, which are not only attributed to intrinsic absorption losses but also to scattering. Finally, misalignment losses were also checked by moving the fiber in the vertical and horizontal direction up to a maximum decay of 1 dB in the measured power. Misalignments of $\pm 2\,\mu$m in the horizontal and vertical directions for guides with 85 %

overlap to the fiber mode confirm the large tolerances expected from input chip waveguides.

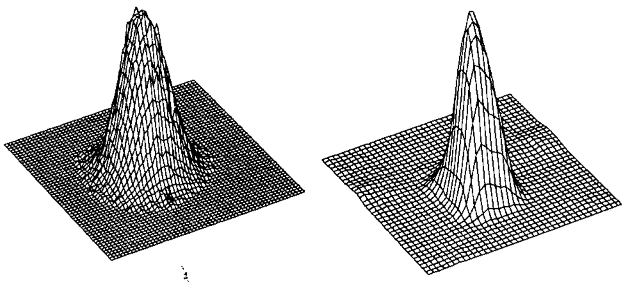

Figure 12 - Measured intensity profiles of the fundamental mode at the output of the glass fiber (left) and of a rib waveguide (right) with an overlap efficiency of $\eta' = 85\%$.

5. Conclusions

Butt joints between single mode fibers and large input waveguides of future photonic integrated circuits made of n^-/n^+-InP layers were investigated theoretically and experimentally. These large waveguides are designed as input sections for integrated optical tapers and fabricated using liquid phase epitaxy and wet chemical etching. In the case of an ideal mode match, theory predictes a maximum coupling efficiency of ca. 86 % between the single-mode fiber and input waveguides, showing losses only due to Fresnel reflections on the interface. Moreover, no theoretical distinction in the coupling efficiency can be made for optimized buried rib and symmetric guides, whose employment in the practice will be given by the degree of difficulty in the fabrication process. Our measured waveguide show a mode mismatch of about $1 - \eta' = 15$ % (0.7 dB) to a single-mode fiber of 9 μm spot diameter. This will give a coupling efficiency of $\eta = 75$ % or 1.25 dB/interface if one takes a reflectance of 14 % at the joint into account. An even better matching to the fiber mode will experimentally be possible if a lower refractive index step is taylored between substrate and guiding layer.

Acknowledgments

We express greatly our thanks to Dr. P. Stuwe for valuable discussions and U. Heydecke, W. Pohlmann and D. Hauschild for technical assistance during the fabrication and measurements of the chip-waveguides.

References

[1] H.-P. Nolting, and C. M. Weinert, "Theoretical Investigations of Optical Waveguide Tapers on InGaAsP/InP", Frequenz, vol. 45, no. 5-6, pp. 130-140, 1991.

[2] P. Stuwe, S.-P. Chen, and T. Schwander, "Low Loss Fiber-Chip Connections with Optimized Butt Joints and a Novel Integrated Optical Taper", Frequenz, vol. 45, no. 9-10, pp. 233-238, 1991.

[3] R. J. Deri and E. Kapon, "Low-loss III-V Semiconductor Optical Waveguides", IEEE J. Quantum Electron., vol. 27, no. 3, pp. 626-640, 1991.

[4] D. Marcuse, "Radiation Losses of Tapered Dielectric Slab Waveguides", Bell Syst. Tech. J., vol. 49, pp. 273-290, Feb. 1970.

[5] P. Stuwe, *Passive Wellenleiterbauelemente fuer den optoelektronisch integrierten Teilnehmeranschluss.* Duesseldorf: VDI Verlag, 1993.

[6] German Norm, *Lichtwellenleiter fuer Fernmelde- und Informationsverarbeitungsanlagen, Teil 2: Faser, Einzeladern und Buendeladern.* DIN VDE 0888, August, 1987.

[7] B. R. Bennet, R. A. Soref and J. A. del Alamo, "Carrier-Induced Change in Refractive Index of InP, GaAs and InGaAsP", IEEE J. Quantum Electron., vol. 26, no. 1, pp. 113-122, 1990.

[8] P. Stuwe, private communication.

[9] J.J. Hsieh, "Thickness and Surface Morphology of GaAs LPE Layers Grown by Supercooling, Step-Cooling, Equilibrium-Cooling, and Two-Phase Solution Techniques", J. Crystal Growth, vol. 27, pp. 49-61, 1974.

[10] W.H. Press, S.A. Teukolsky, W.T. Vetterling, and B.P. Flannery, *Numerical Recipes in FORTRAN, The Art of Scientific Computing.* New York: Cambridge University Press, 1992.

[11] D. Botez, "Liquid-Phase Epitaxy over Channelled Substrates", J. of Cryst. Growth, vol. 70, pp. 150-154, 1984.

[12] A. Pohl, H. Fouckhardt, and H.-G. Unger, "Symmetrical Field-Matching Waveguide For Low-Loss Fiber-Chip Butt Coupling", J. Opt. Communications, vol. 16, no. 4, pp. 138-142 (1995).

[13] E.J. Murphy, T.C. Rice, L. Mccaughan, G.T. Harvey, and P.H. Read, "Permanent Attachment of Single-Mode Fiber Arrays to Waveguides", J. of Lightwave Techn., vol. LT-3, no. 4, pp. 795-799, 1985.

[14] E. J. Murphy, "Fiber Attachment for Guided Wave Devices", J. Lightwave Technol., vol. 6, no. 6, pp. 862-871, 1988.

[15] K. Kasaya, O.Mitomi, M. Naganuma, Y.Kondo, and Y. Noguchi, "A Simple Laterally Tapered Waveguide for Low-Loss Coupling to Single-Mode Fibers", IEEE Photon. Technol. Lett., vol. 5, no. 3, pp. 345-347, 1993.

[16] R. Zengerle, H. Brückner, H. Olzhausen, and A. Kohl, "Low-Loss Fibre-Chip Coupling by Buried Laterally Tapered InP/InGaAsP Waveguide Structure", Electron. Lett., vol. 28, no. 7, pp. 631-632, 1992.

[17] R.J. Deri, "Efficient Fiber Coupling to Low-Loss Diluted MQW Optical Waveguides", Appl. Phys. Lett., vol. 55, no. 15, pp. 1495-1497, 1989.

[18] R. G. Hunsperger, *Integrated Optics: Theory and Technology*. Berlin-Heidelberg: Springer-Verlag, 1982.